NJC

New Journal of Chemistry

A journal for new directions in chemistry

Accepted Manuscript

This article can be cited before page numbers have been issued, to do this please use: B. Sun, K. Cheng, C. X. Ling, D. Gu, Z. Gao, Y. Li, P. An, Y. Zhang, C. You and R. Zhang, *New J. Chem.*, 2020, DOI: 10.1039/C9NJ05469C.

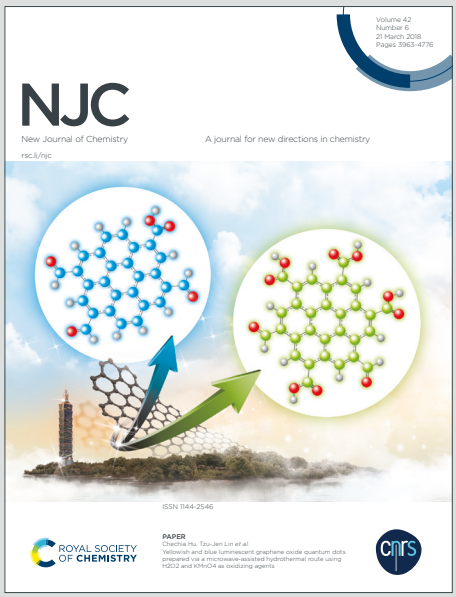

This is an Accepted Manuscript, which has been through the Royal Society of Chemistry peer review process and has been accepted for publication.

Accepted Manuscripts are published online shortly after acceptance, before technical editing, formatting and proof reading. Using this free service, authors can make their results available to the community, in citable form, before we publish the edited article. We will replace this Accepted Manuscript with the edited and formatted Advance Article as soon as it is available.

You can find more information about Accepted Manuscripts in the Information for Authors.

Please note that technical editing may introduce minor changes to the text and/or graphics, which may alter content. The journal's standard Terms & Conditions and the Ethical guidelines still apply. In no event shall the Royal Society of Chemistry be held responsible for any errors or omissions in this Accepted Manuscript or any consequences arising from the use of any information it contains.

View Article Online
DOI: 10.1039/C9NJ05469C

Multimodal therapies: Glucose Oxidase-triggered Tumor Starvation Induced Synergism with Enhanced Chemodynamic Therapy and Chemotherapy

Kaiwu Cheng[a], Chuxuan Ling[a], Dihai Gu[a], Zhiguo Gao[a], Yaojia Li[a], Peijing An[a], Yu Zhang[a], Chaoqun You[c], Rui Zhang[b,] *, Baiwang Sun[a,] *.

[a] School of Chemistry and Chemical Engineering, Southeast University, Nanjing 210089, PR China. Fax: +86 25 52090614, Tel: +86 25 52090614, *E-mail address: chmsunbw@seu.edu.cn

[b] Department of Ophthalmology, Zhongda Hospital, Southeast University, Nanjing 210009, China.

[c] College of Chemical Engineering, Nanjing Forestry University, Nanjing 210037, PR China

Abstract

Tumor microenvironment are distinct from normal tissue cells in characteristic physiochemical conditions, based on which we could design tumor-specific therapy modality. Herein, we introduce a concept of multimodal therapies, which integrates the characteristics of each therapy modality, for efficient tumor therapy: tumor starvation triggered synergism with enhanced chemodynamic therapy and activated chemotherapy. Fe_3O_4 nanoparticles (Fenton reaction catalyst) and a hypoxic prodrug of tirapazamine (TPZ) were loaded in mesoporous silica nanoparticles (MSN) and GOX was grafted onto its surface, which was designed and fabricated for the sequential multimodal therapies. Logically, Glucose oxidase (GOX) deprives tumor cells of nutrients (glucose and oxygen) for starvation therapy and tumorous abnormality amplifications (elevated acidity, exacerbated hypoxia and increased H_2O_2) was amplified by the GOX-driven oxidation reaction simultaneously. Specifically, elevated acidity could accelerate the release of iron ion and enhanced Fenton reaction efficiency. Associated with the

increased H_2O_2, elevated ROS level was detected that enhanced chemodynamic therapy. Exacerbated hypoxia activated the hypoxic prodrug (TPZ) for tumor-specific chemotherapy programmatically. Particularly, integrated starvation therapy, enhanced chemodynamic therapy and activated chemotherapy, the sequential multimodal therapies was specifically designed for the tumor microenvironment and achieved effective abnormality amplifications and high therapeutic efficacy.

Key words: multimodal therapies, Glucose oxidase, chemodynamic therapy, Fenton reaction, starvation therapy

Introduction

Cancer remains the most fatal diseases in the world and conventional therapeutic modalities including toxic chemotherapeutics, invasive surgical treatment and external high-energy irradiations merely achieve limited results with severe adverse effects inevitably[1–3]. Monotherapy is difficult to achieve the desired therapeutic effect due to multiple pathways in tumor pathogenesis. Therefore, Multimodal therapies integrateing the characteristics of each therapy modality has been proposed currently for efficient tumor therapy, which promotes the synergy of various monotherapy[4–6]. Particularly, tumor microenvironment is different from normal tissue in pH value, redox elevation, hypoxia, enzyme overexpression[7]. Nevertheless, these abnormalities are inadequate for cancer cell with tumor-specific therapy effectively. Therefore, therapy modality designed for expanding and responding specifically to tumor heterogeneity would reduce tumor resistance while reducing toxic side effects on normal tissues. Reactive oxygen species (ROS) including superoxide anion radicals ($O_2^{-\bullet}$), singlet oxygen ($^1O_2$) and hydroxyl radicals (•OH) are essential in normal metabolic activity for normal cells at low levels[8–11]. While high level ROS could destroy cells by oxidizing intracellular glutathione, DNA, protein and lipid[12–14]. Chemodynamic therapy (CDT) was known for its unique way of generating ROS independent of local oxygen in recent years.

View Article Online
DOI: 10.1039/C9NJ05469C

Produced by endogenous H_2O_2 through a metal ion-mediated Fenton reaction[15], •OH have received the most extensive attention for its powerful oxidizing capacity, resulting in fatally damage to tumor cells[16]. Although chemodynamic therapy exhibits advantages over traditional therapy models such as nonspecific side effects of extensive chemotherapy and low efficiency (oxygen dependence and restricted light penetration) of photodynamic therapy[17]. Regrettably, CDT depends on high efficiency catalyst and highly concentrated H_2O_2 in vivo.

Nowadays, various transition metal ions like Cu(II) and Mn(II) have been applied as catalyst to initiate a Fenton-like reaction for CDT[18], while the most widely used is still Fe(II), commonly coming from Ferromagnetic nanoparticles (Fe_3O_4 NPs)[19,20]. Shi et al. introduced Fe_3O_4 nanoparticles into large pore-sized and biodegradable dendritic silica nanoparticles to catalyze intracellular H_2O_2 for high level of ROS[15]. H_2O_2 concentration is intrinsically higher than normal physiological environment at tumor tissue, yet still insufficient for highly efficient and specific CDT[21,22]. In order to obtain adequate H_2O_2, strategies like introducing exogenous H_2O_2 or stimulating the production of endogenous H_2O_2 were put forward in response to the issue of insufficient endogenous H_2O_2. Glucose oxidase (GOX, natural enzyme catalyst) has been introduced to tumor therapy by triggering starvation therapy through consuming oxygen and β-D-glucose to generate gluconic acid and H_2O_2[6,23]. Simultaneously, due to the distinct metabolic process, tumor cells demand more glucose for glycolysis to support its endless proliferate, which would provide abundant H_2O_2 and acidity[4], resulting in exacerbated hypoxia at the same time[24]. Most importantly, tumorous abnormality and heterogeneity amplifications create opportunities for sensitized chemotherapy especially for a hypoxic-responsive tirapazamine (TPZ)[25], which would be fatal to anoxic tumor cells, but safe for oxygen-sufficient normal cells[26]. Chemotherapy usually could not achieve desired therapeutic effect due to multidrug resistance (MDR) effect of cancer[27]. And nonspecific and inaccurate injure to normal cells, poor solubility and rapid blood clearance also restrict its further development in clinical research[28–30].

View Article Online
DOI: 10.1039/C9NJ05469C

Aiming at above challenges, 'intelligent' drug delivery systems (DDSs) have been designed for delivering biocompatible anticancer drugs carrier to tumor sites[31,32], among which mesoporous silica nanoparticles (MSNs) have got far-reaching attention and applications owing to its outstanding properties including well biocompatibility[7], highly drug loading capacity, tunable particle size, well-defined mesoporous and especially, easily functionalized surface[33–35]. However, the multiple pathways and heterogeneity involved in the pathogenesis of the tumor restrict the therapeutic effect of monotherapy[36]. In this paper, multimodal therapies (tumor starvation therapy triggered synergism with chemodynamic therapy and sensitized chemotherapy) was reported for the efficient oncotherapy and summary synthesis of TPZ/Fe_3O_4@MSN-GOX was shown in **Scheme 1**. Hypoxic-responsive Tirapazamine (TPZ) and high efficiency catalyst Fe_3O_4 were enveloped in biocompatible MSN with GOX grafted on its surface. Logically, GOX deprived tumor cells of nutrition (oxygen and glucose) for starvation therapy and induced tumorous heterogeneity amplifications[4] (increased H_2O_2, decreased acidity and anabatic hypoxia), which activated the sensitized chemotherapy under hypoxia and triggered chemodynamic therapy with the participation of Fe_3O_4 and GOX-metabolite (H_2O_2 and H^+) simultaneously. Meanwhile, external GOX also served as a guard to protect the premature release of TPZ. Fe_3O_4 nanoparticles was translated into Fe^{2+}/Fe^{3+} in acid environment, which catalyzed abundant intracellular H_2O_2 into highly toxic hydroxyl radical (•OH) for highly efficient CDT. Synergetic multimodal therapies achieved satisfactory antitumor effect in vitro.

View Article Online
DOI: 10.1039/C9NJ05469C

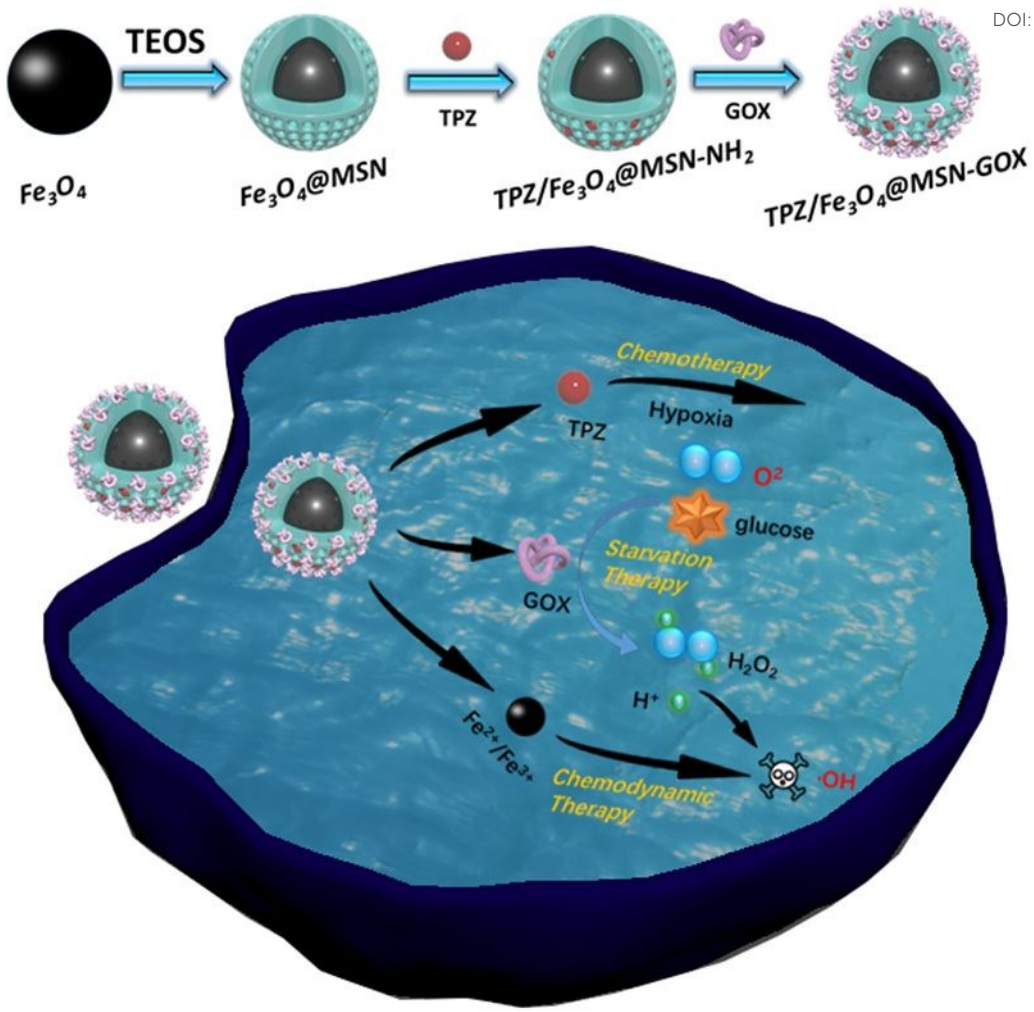

Scheme 1. Schematic illustration of the synthesis of TPZ/Fe_3O_4@MSN-GOX and GOX triggerred hunger treatment, sensitized chemotherapy and chemodynamic therapy for efficient multimodal tumor treatment.

2. Materials and methods

2.1. Materials

Tetraethylorthosilicate (TEOS), ammonia solution (25-28%), sodium carbonate (Na_2CO_3), diethyl ether, Cetyltrimethylammonium bromide (CTAB), dimethyl sulfoxide (DMSO), hydrochloric acid (HCl) and ethanol were purchased from Sinopharm chemical reagent Co., Ltd (Shanghai, China). TPZ was provided by Dalian Meilun Biotech Co., Glucose oxidase (GOX) were purchased from GIBCO

Invitrogen Corp. (Carlsbad, USA). 3-aminopropyltriethoxysilane (APTES), 2, 2-dithiodipyridine, and tirapazamine were purchased from Aladdin Reagent Co., Ltd (Shanghai, China). Molecular probe 2-(4-amidinophenyl)-6-indolecarbamidine dihydrochloride (DAPI) was obtained from Beyotime Biotechnology (China), annexin V-FITC/PI apoptosis was purchased from 4A Biotech Co., Ltd. (Beijing, China). Fetal bovine serum (FBS), Dulbecco's modified Eagle's medium (DMEM), All other reagents were of analytical grade and used as received.

2.2. Preparation of TPZ/Fe_3O_4@MSN-GOX

2.2.1 Synthesis of the Fe_3O_4

Magnetic core was prepared via the thermal decomposition of iron oleate according to the literature with some modifications. Briefly, Dissolving Iron(III) chloride hexahydrate ($FeCl_3$•$6H_2O$, 5.4 g) and 17 mL oleic acid in 100 mL of methanol. Next, adding 200 mL 0.3M NaOH thereto with stirring and washed product three times before vacuum drying. Finally, iron oleate was obtained. 31.0g 1-octadecene and 5.5g iron oleate were stirred at 65℃. And adding 1.5 g oleic acid and then vigorous stirred at 320℃ for 0.5h under nitrogen atmosphere. 40 mL of ethanol was added into thereto and shook vigorously after cooling down. Then products were obtained by centrifugation at 8000 rpm and washed with 40 mL of acetone/hexane (3:1) three times by centrifugation. At last, dispersing the Fe_3O_4 nanoparticles in chloroform at a concentration of 23.2 mg Fe_3O_4 per mL.

2.2.2 Synthesis of Fe_3O_4@MSN nanoparticles

The Fe_3O_4@MSN nanoparticles were prepared via a modified sol-gel method[37]. Firstly, 440 μL 2M NaOH and 125 mg of CTAB were dissolved in 60 mL of deionized water, heated to 70℃ for 1.5h under vigorous stirring. Then, 1 mL of Fe_3O_4 nanoparticles solution with evenly distributed was added and chloroform was removed by continuous nitrogen stream. Then, the solution was stirred at 80℃ for 1h and 200 mL of TEOS was added for mixture. At last, an additional 400 mL of TEOS was added thereto and the

reacted at 80℃ for 1.5 h. The precipitate was collected by centrifugation and washed with deionized water and ethanol respectively three times before vacuum drying. Refluxed for 6 h in 90 mL ethanol solution of NH_4NO_3 (6 mg/mL) twice, Fe_3O_4@MSN without CTAB template was obtained after washed with deionized water and ethanol respectively three times before vacuum drying.

2.2.3 Synthesis of Fe_3O_4@MSN-NH_2 nanoparticles

250mg of Fe_3O_4@MSN and 1.2 mL of APTES were mixed and refluxed in 50 mL anhydrous toluene for 24 hours. Then, the precipitate was collected via centrifugation at 12000 rpm for 15 min. Finally, Fe_3O_4@MSN-NH_2 nanoparticles was obtained by washing collected product with deionized water and ethanol respectively three times and dried overnight under vacuum.

2.2.4 Drug loading and GOX capping

Dispersing 20 mg of TPZ and 40 mg Fe_3O_4@MSN-NH_2 in 10mL PBS (pH=7.4) and stirred for 24 h, collected by centrifuged and washed. Additionally, dispersing 58 mg of EDC·HCl, 88 mg of NHS in 12 mL of deionized water and stirred for 20 min at room temperature, followed with 10 mg of GOX, stirred for 8 hours, and finally 50 mg TPZ/Fe_3O_4@MSN-NH_2 was added. Subsequently, the TPZ/Fe_3O_4@MSN-GOX was collected via centrifuging at 12000 rpm for 10 min, then washed by deionized water ethanol orderly and dried overnight in vacuum.

2.3. Characterizations

Scanning electron microscopy (SEM) (FEI Inspect F50) and JEM-100CXII transmission electron microscopy (TEM) were employed to analyze the morphology of Fe_3O_4 NPs and Fe_3O_4@MSN. The surface area and pore size distribution were measured by nitrogen (N_2) adsorption-desorption method on a Brunauer-Emmett-Teller Micromeritics Thristar 3000 analyzer. FTIR and UV-vis adsorption were respectively performed on a Thermo Scientific Nicolet 6700 FTIR spectrometer (Asheville, NC, USA) and UV-2600 (Shimadzu, Japan). Dynamic light scattering (DLS) was employed

to analyze zeta potential and hydrodynamic size of Fe_3O_4@MSN on a Malvern Zetasizer NanoZS (UK) instrument. Thermogravimetric analysis (TGA) was conducted on TG209 F3 thermogravimetric analyzer (NETZSCH, Germany) with a heating rate of 10°C/min in a nitrogen stream. PPMS-9 (Quantum Design) and ICP-MS 7400 (Thermo Fisher Scientific) were used to detect Hysteresis loops and iron masses respectively.

2.4. The magnetism of Fe_3O_4 NPs and Fe_3O_4@MSN

Hysteresis loops of Fe_3O_4 and Fe_3O_4@MSN nanoparticles were investigated by superconducting quantum interference device vibrating sample magnetometer (SQUID, Quantum Design MPMS) in previous work[8], which had superior magnetic properties and exhibited magnetic targeting potential in clinic.

2.5. Iron ion responsive release

Ferric ion was detected by dialysis method, each sample in triplicate. Briefly, 25 mL of 1 mg/mL TPZ/Fe_3O_4@MSN-GOX were dispersed in PBS solutions (pH =5.0, 7.4) with or without glucose (1 mg/mL) then all solutions were stirred (100 rpm) at 37 °C in the dark. At given intervals (0h, 1h, 2h, 4h, 8h, 12h, 24h, 36h, 48h),1 mL of the releasing buffer was taken out and equal dosage of fresh buffer was replenished. After 15min four systems were added with KSCN (10 mg/mL) respectively. At last, the UV-vis absorption was quantitatively measured by standard curve at 478 nm and the iron ion released also could be observed according to their color.

2.6. Drug loading capacity

Dispersing TPZ/Fe_3O_4@MSN-GOX in 20 mL of PBS (pH = 7.4) and stirred in the dark at 25°C for 15h. Then the supernatant was removed by centrifuged, and the remaining solid was dispersed in deionized water uniformly. All the cleaning liquid fractions were collected according to the previous method[38], all collected supernatant containing TPZ and GOX detected by using a standard curve via UV-vis adsorption at 262 nm and 280nm respectively with a standard curve. Drug loading content (DLC) was determined

View Article Online
DOI: 10.1039/C9NJ05469C

by equations.

$$\text{DLC (wt \%)} = \frac{weight\ of\ \ TPZ\ in\ nanoparticles}{weight\ of\ \ nanoparticles}$$

The amount of GOX was determined by the difference in mass loss of Fe_3O_4@MSN and Fe_3O_4@MSN-GOX on the thermogravimetric analyzer (TGA).

A standard inductively coupled plasma mass spectrometry (ICP-MS) procedure was conducted to quantify the amount of Fe_3O_4 nanoparticles in triplicate. Briefly, 1 mg of TPZ/Fe_3O_4@MSN-GOX and TPZ/Fe_3O_4@MSN were dissolved into 10 mL deionized water followed by measurement of ICP-MS.

$$\text{DLC (wt \%)} = \frac{weight\ of cargos(Fe3O4\ NPs)}{weight\ of\ nanoparticles}$$

2.7. The stability of TPZ/Fe_3O_4@MSN-GOX in vitro

The prepared TPZ/Fe_3O_4@MSN-GOX was kept at 4°C for 4 weeks to study its stability. All samples were stirred and purified by a 0.45 μm filter[34]. Changes in PDI and size were assessed its stability by specific time intervals (0, 1, 2, 3, 4 weeks). 5 mg of TPZ/Fe_3O_4@MSN-GOX was dispersed in 50 mL PBS (pH=7.4) solution and fetch 2 mL of TPZ/Fe_3O_4@MSN-GOX solution, treat with ultrasound for 5 min followed with DLS test in triplicate at each scheduled time.

2.8. GOX reduces pH and promote H_2O_2 in vitro

GOX could reduce pH and elevate H_2O_2 concentration has been reported in previous work[39]. GOX, Fe_3O_4@MSN, Fe_3O_4@MSN-GOX at specific concentration intervals (800 μg/mL, 400 μg/mL, 200 μg/mL,100 μg/mL, 50 μg/mL, 0 μg/mL) were dispersed in PBS (pH=7.4) with or without glucose (1 mg/mL) and incubated 4 hours in the dark at 37°C. pH was detected by Orion portable pH meter (Orion 8103BN ROSS semi-micro pH electrode, Boston, MA, USA) and H_2O_2 concentration was determined by the specific ultraviolet absorption of yellow titanium peroxide complex ($Ti(IV)O_2^{2+}$) arising from the reaction of the colorless $Ti(IV)O^{2+}$ and H_2O_2[23]. In addition, all samples were in triplicate.

View Article Online
DOI: 10.1039/C9NJ05469C

2.9. In vitro drug release

The drug release of TPZ/Fe_3O_4@MSN-GOX was conducted in PBS (pH =7.4, pH=5.0) with glucose (1 mg/mL) or without glucose by using a dialysis method.[40] Equal amount of TPZ/Fe_3O_4@MSN and TPZ/Fe_3O_4@MSN-GOX were transferred into dialysis bags (MWCO 10 kDa) and soaked and stirred in 25 mL of PBS (pH =7.4, pH=5.0) at 37 °C in the dark, and 2 mL of the buffer solution was taken at a specific interval (1 h, 2 h, 4 h, 8 h, 12h, 24 h, 48 h) to investigate the release concentration of TPZ, and equal dosage of PBS solution was replenished. The release mass of TPZ was calculated by comparing the specific UV-vis adsorption with a standard curve.

2.10. Detection of hydroxyl radicals

Methylene blue (MB) was typical indicator of •OH, which could degrade methylene blue by its strong oxidizing and could quantitative detected by UV-Vis absorption. Dispersing 1 mg Fe_3O_4@MSN, Fe_3O_4@MSN-GOX in 25 mL PBS (pH=7.4) containing 10 μg/mL methylene blue, 8 mM H_2O_2 with or without glucose (1 mg/mL) and stirred for 30 min. The ·OH produced by Fe_3O_4-mediated Fenton reaction could degrade methylene blue and detected by absorbance change at 665 nm.

2.11. Cell culture

Human breast cancer cells MCF-7 and normal liver cells L-02 were selected and incubated in RPMI-1640 complete medium containing 10% FBS and 1% penicillin-streptomycin solution, which were cultured in a humidified atmosphere at 37°C containing 5% CO_2.

2.12. Cellular uptake

Confocal laser scanning microscope (CLSM, Zeiss, Germany) was applied to determine the cellular uptake efficiency of TPZ/Fe_3O_4@MSN-GOX. 1×10^5 MCF-7 cells per well were incubated at 37°C in a confocal petri dish (BD Falcon, USA) for 12 hours. Then dispersing TPZ/Fe_3O_4@MSN-GOX uniformly in the RPMI-1640 complete medium and then incubated at predetermined time intervals (1h, 4h, 8h) at 37°C. Next, all cells

were washed three times with PBS and then fixed with 4% paraformaldehyde for 15 minutes[41], then followed by washing three times with PBS and 150 μL of DAPI (100 ng/mL) was added to the medium[1]. Finally, the cellular uptake was observed and assessed via CLSM.

2.13. Detection of reactive oxygen species (ROS)

The generation of intracellular ROS was detected by a DCFDA assay. MCF-7 cells (1 × 10^5 cells per well) were seeded in confocal Petri dishes (BD Falcon, USA) containing glucose (1 mg/mL) at 37°C for 24 h and incubated with TPZ/Fe_3O_4@MSN-GOX and TPZ/Fe_3O_4@MSN for different incubation times (1h, 4h, 8h). The cells were washed three times with PBS after incubation and stained with 1 mL of DCFDA (10 mM) for 20 min, which was observed by CLSM after washed with PBS.

2.14. In vitro cytotoxicity test

MTT assays were applied to determine the cytotoxicity of different particles against MCF-7 cells and L-02 cells at 6.0 × 10^3 cells/well into 96-well plates. Starvation therapy was conduct at the glucose-containing and glucose-free DMEM media. Then 100 μg/mL, 200 μg/mL Fe_3O_4@MSN-GOX were added to each well and co-incubation, at last MTT assays was used to evaluated viability. After incubated with RPMI-1640 complete medium (100 μL) for 24 hours, L-02 cells were incubated in a normoxic (20% O_2) environment with blank MSN at different concentrations (3.12, 6.25, 12.5, 25, 50, 100, 200 μg/mL) to test the biocompatibility of MSN and incubated with free TPZ, TPZ/Fe_3O_4@MSN and TPZ/Fe_3O_4@MSN-GOX with different concentrations (0.5, 1, 2, 4, 8, 16 μg/mL) to test their toxicity to normal cells. Subsequently, TPZ dose-dependent concentrations (0.5, 1, 2, 4, 8, 16 μg/mL) of free TPZ, TPZ/Fe_3O_4@MSN and TPZ/Fe_3O_4@MSN-GOX under different O_2 concentrations were co-cultured with MCF-7 cells into in glucose-containing (1 mg/mL) media. Before adding fresh 200 μL DMEM medium to each well, all cells were cleared with 200 μL PBS and then cultured for 24 hours in a normoxic (20% O_2) and hypoxic (5% O_2) environment at 37°C, and each well was rinsed. Next, 150 μL complete medium containing 20 μL of MTT was

added thereto and incubated for 4 hours. 180 μL of DMSO was added to replace previous medium each well in the 96-well plate[8], which then shaken on a benchtop concentrator for 15 minutes[42]. At last, plate reader Spectra Max Microplate Reader (Sunnyvale, CA, US) was used for measurements.

2.15. Cell apoptosis

Cell apoptosis was detected by Annexin APC/7-AAD Apoptosis Detection Kit II (BD Pharmingen, San Jose, USA). Briefly, the same TPZ dosage of 40 μg/mL free TPZ, TPZ/Fe_3O_4@MSN and TPZ/Fe_3O_4@MSN-GOX were added into 6-well plates, which were seeded at 1.0×10^5 cells/well and cultured in a normoxic (20% O_2) and hypoxic (5% O_2) environment at 37°C. Control group was conducted with 40 μg/mL MSN co-cultured. The medium was removed after 12h followed with all cells washed three times and digested with 1.0 mL of EDTA-free trypsin. The cells were collected and dispersed uniformly in 500 μL buffer, and then 5 μL of propidium iodide and 5 μL of Annexin V-FITC were added thereto in the dark to stain the cells for 15 minutes. At last, all samples were analyzed by flow cytometry on a FACS Calibur (BD Biosciences, USA).

3. Results and discussion

3.1 Synthesis and characterization of Fe_3O_4@MSN-GOX

In this work, core-shell structured Fe_3O_4@MSN-GOX were fabricated by the procedures illustrated in **Scheme 1**. As the core, Fe_3O_4 nanoparticles were obtained by thermal decomposition method, with hydrophobic and monodisperse morphology, whose diameter size was about 8 nm showed **in Figure 1(a)**. As the shell, the mesoporous silica was coated onto the Fe_3O_4 NPs by a traditional Stöber method. GOX was grafted on the surface of Fe_3O_4@MSN to block off the mesoporous. Fe_3O_4@MSN exhibited uniform nanospheres with diameter size of 55 nm, which were observed by

TEM and SEM in **Figure 1(b)** and **(c)**. In addition, in **Figure 3(a)** and **Figure 6(d)**, polydispersity index (PDI) value and hydrodynamic size of Fe_3O_4@MSN were about 0.154 and 88 nm respectively, owing to the exterior hydration layers. According to **Figure 2(a)** and **(b)**, N_2 adsorption-analytical analysis result revealed that the highly surface area and uniform, defined pore size of Fe_3O_4@MSN were 517.4 m^2g^{-1} and 2.6 nm respectively.

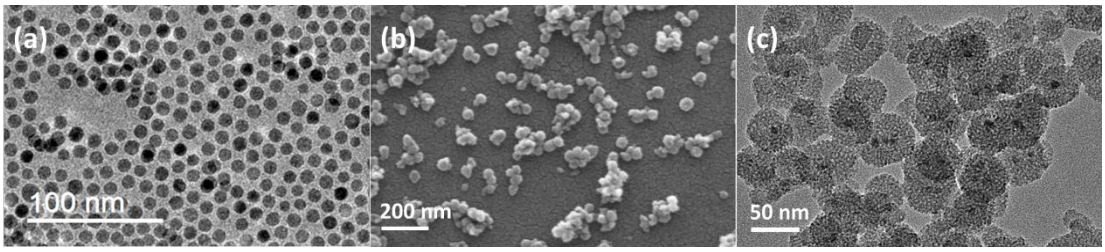

Figure 1. (a) TEM images of Fe_3O_4, (b)SEM image and (c) TEM images of Fe_3O_4@ MSN.

The modification of GOX onto the surface of Fe_3O_4@MSN was verified by zeta potential, FTIR and TGA. The distinct change of zeta potential value of nanoparticles suggested the successful modification in **Figure 3(c)**. The zeta potential of Fe_3O_4@MSN (-25.3 mV) and Fe_3O_4@MSN-NH_2 (17.5 mV) occurred sharp reversed owing to the typical positive charge of -NH_2. After modification with GOX, Fe_3O_4@MSN received negative zeta potential (-9.8 mV). FTIR spectra could be served to prove successful synthesis of materials. According to **Figure 3(b)**, The iron-oxygen bond vibration, Si-O and C=O from oleic acid were reflected by the signals of 580 cm^{-1}, 475 cm^{-1} and 1648 cm^{-1} in FTIR, which could confirm the formation of inner ferric oleate and outer MSN. The peak at 1388 cm^{-1} in Fe_3O_4@MSN-GOX was weaker than in Fe_3O_4@MSN, attributed to the plentiful -CH_3 of tetraethyl orthosilicate (TEOS). The peaks at 1550 cm^{-1}, 1445 cm^{-1} in Fe_3O_4@MSN-GOX were originated form the vibration of C-N and -NH_2 respectively, attributed to the -NH_2 come from GOX. The weight loss value of Fe_3O_4@MSN and Fe_3O_4@MSN-GOX were respectively 21.62% and 27.22%,

View Article Online
DOI: 10.1039/C9NJ05469C

which could quantitatively calculate the amount of GOX (5.6%) according to **Figure 3(d)**.

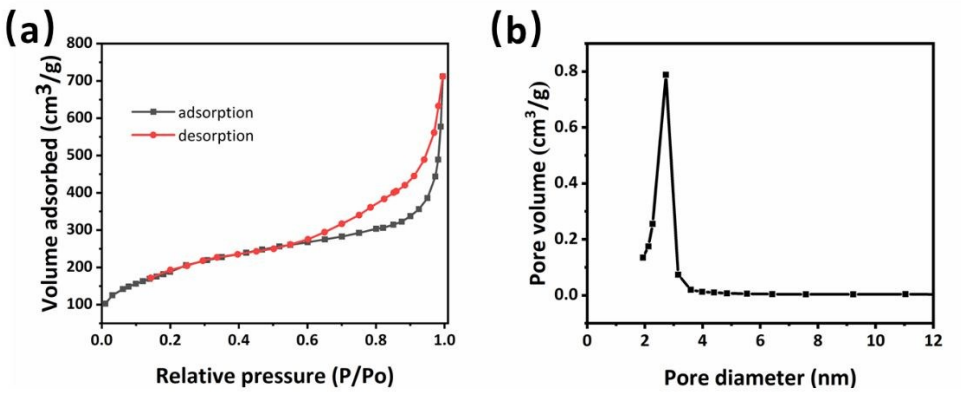

Figure 2. (a) Nitrogen adsorption/desorption isotherm and (b) the pore size distribution of Fe_3O_4@MSN.

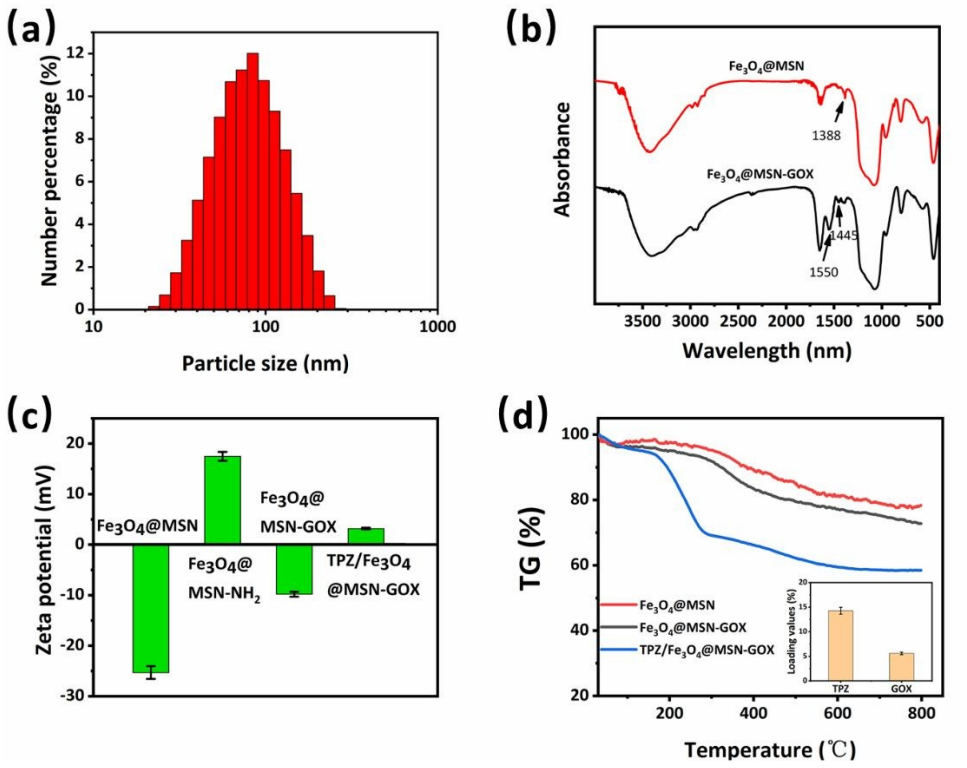

Figure 3. Related characterization of nanoparticle including (a) hydrodynamic diameter size of Fe_3O_4@MSN, (b) FTIR spectra of Fe_3O_4@MSN and Fe_3O_4@MSN-GOX, (c) Zeta potential of Fe_3O_4@MSN, Fe_3O_4@MSN-NH_2, Fe_3O_4@MSN-GOX, TPZ/Fe_3O_4@MSN-GOX and (d) thermogravimetric analysis of Fe_3O_4@MSN,

View Article Online
DOI: 10.1039/C9NJ05469C

Fe_3O_4@MSN-GOX, TPZ/Fe_3O_4@MSN-GOX.

3.2. Ferric ion release

The determination of the iron ion content in the nanoparticles is a prerequisite for evaluating the effect of the Fenton reaction. The mass of iron in Fe_3O_4@MSN and Fe_3O_4@MSN-GOX were 35.14 μg mg^{-1} and 33.15 μg mg^{-1} respectively determined by ICP-MS, which was shown in **Figure 4**. The iron content declined slightly in Fe_3O_4@MSN-GOX compared with Fe_3O_4@MSN, which also confirmed the successful modification of GOX. Due to the complexity and variability of the tumor microenvironment, we conduct the ferric ion release in vitro for simulating the tumor microenvironment. $Fe(SCN)_3$ was formed when ferric ions encountered thiocyanate and specific ultraviolet absorption (**Figure S1(c)**) was detected at 478 nm. The blood red solution gradually deepened as the acidity decreased that indicate the lowed pH could accelerate the release of ferric ions. Different organelles have different pH values in the tumor, such as endosomes (5.0–6.5) and lysosomes (4.5–5.0). However, GOX carried on the surface of the nanoparticles could further reduce the acidity by oxidizing glucose, which was confirmed by previous work[39]. After disposed sample with 1h, the blood red solution also deepened as glucose concentration increased and the reduced pH also increased the of release of ferric ion in **Figure 5(a)**. Low pH could promote the dissolution of Fe_3O_4 to release ferric ion, which served as efficient catalyst for Fenton reactions. The relevant UV quantitative analysis of prepared nanoparticles ferric ions release with time was shown in **Figure 5(b)**. As revealed by the results, GOX can rely on the metabolism of glucose to reduce the pH of the system, thereby accelerate the release of iron ions, thus provide highly efficient catalyst for the Fenton reaction.

View Article Online
DOI: 10.1039/C9NJ05469C

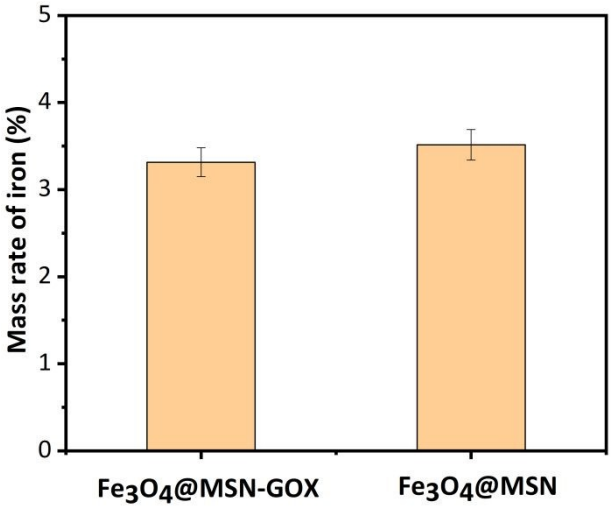

Figure 4. The mass rate of iron in Fe_3O_4@MSN and Fe_3O_4@MSN-GOX.

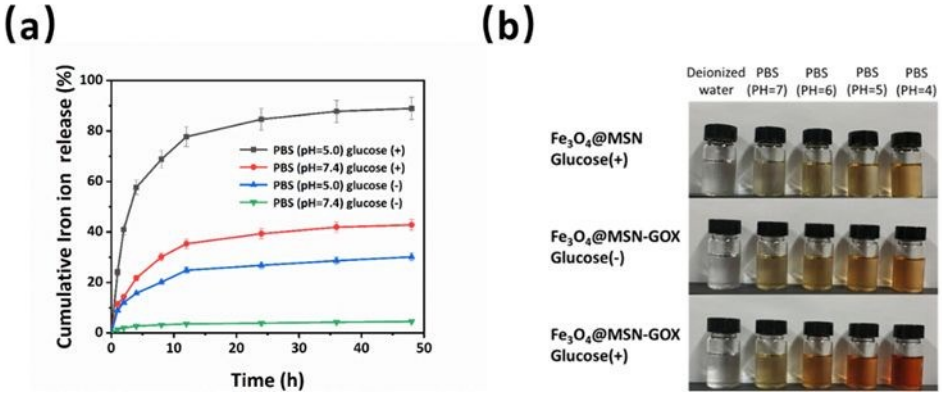

Figure 5. (a) Ferric ions release of TPZ/Fe_3O_4@MSN-GOX over time in PBS (pH=5.0, pH=7.4) with or without glucose (1 mg/mL) and (b) Color changes of Fe_3O_4@MSN and Fe_3O_4@MSN-GOX in PBS at different pH values with or without glucose (1 mg/mL).

3.3. The stability of TPZ/Fe_3O_4@MSN-GOX and in vitro drug release

Drug loading rate of TPZ/Fe_3O_4@MSN-GOX was investigated by UV-vis adsorption peak at 262 nm for TPZ, which were quantitatively calculated and the amounts were 14.9% of TPZ. Respectively, the content of GOX was 5.8% which was determined by the more accurate the BCA Protein Assay Kit (**Figure S4**). UV-vis adsorption and

standard curves of TPZ were shown in **Figure S1(b)**. Furthermore, loading rate of TPZ and GOX were also determined by comparing the weight loss value of TPZ/Fe_3O_4@MSN-GOX (58.51%), Fe_3O_4@MSN-GOX (72.78%) and Fe_3O_4@MSN (78.30%) in **Figure 1(f)**. Prepared nanoparticles were stored at 4°C for 14 days in the PBS (pH = 7.4) for the evaluation of the stability and the index of PDI and particle size were shown in **Figure 6(d)**. The PDI and particle size remained general stable with only minimal fluctuations around 0.154 and 88 nm, which proved the admirable stability of the nanoparticles at 4°C. Drug release experiments were studied in PBS (pH = 5.0, glucose (1 mg/mL)), PBS (pH = 7.4, glucose (1 mg/mL)), PBS (pH = 5.0) and PBS (pH = 7.4) by dialysis method in **Figure 6(c)**. In weak acid environment without glucose, the release of TPZ (29.4%) was faster than that in neutral environment (3.5%) without glucose within 48h. And drug release could be accelerated ((pH = 5.0, 59.3%; pH = 7.4, 43.8%) with the presence of glucose (1 mg/mL). The result suggested that in the tumor microenvironment, weak acid and abundant glucose would promote drug release. However, TPZ/Fe_3O_4@MSN-GOX would further reduce acidity by catalyzing the oxidation of glucose.

3.4. GOX reduces pH and promotes H_2O_2 in vitro

GOX could raise H_2O_2 levels and lower pH by oxidizing glucose and the quantitative analysis results were shown in **Figure 6(a)** and **(b)**. In the groups of GOX and Fe_3O_4@MSN-GOX, reduced pH and elevated H_2O_2 concentration were detected in PBS containing glucose (1 mg/mL) after 4h, there was no apparent change in PBS without glucose. However, In the group of Fe_3O_4@MSN, regardless of whether or not glucose was contained, there was no change in pH and H_2O_2 level. The result could explain the effects of GOX on lowering pH and elevating H_2O_2, further demonstrates the feasibility of hunger treatment and chemodynamic therapy therapy.

View Article Online
DOI: 10.1039/C9NJ05469C

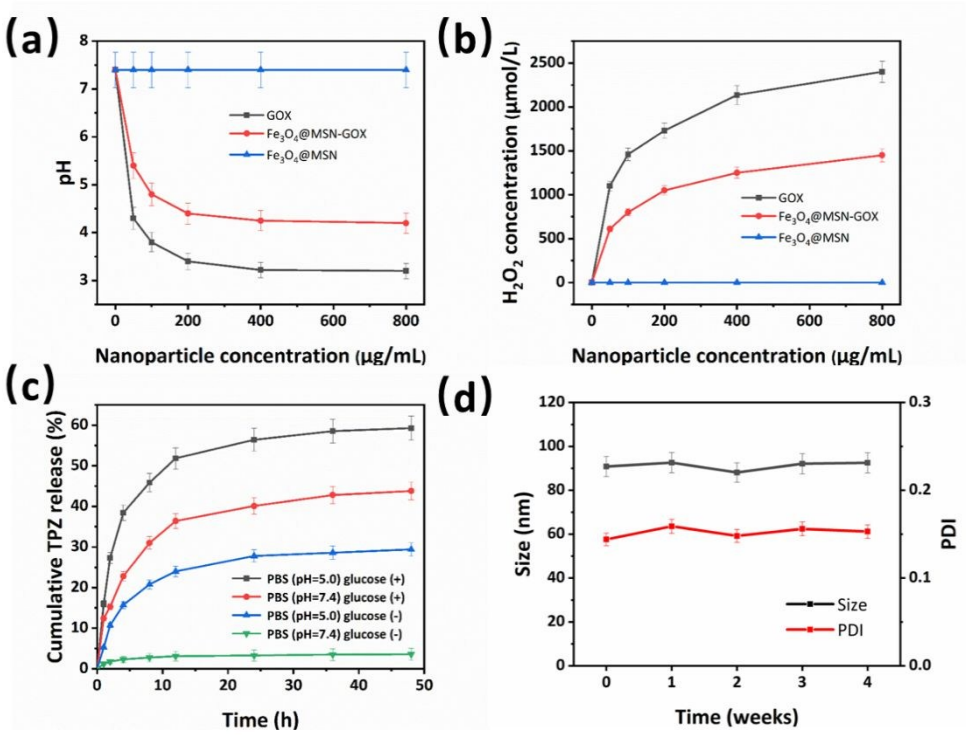

Figure 6. Changes of (a)pH and (b)H_2O_2 concentration of GOX, Fe_3O_4@MSN and Fe_3O_4@MSN-GOX in PBS (pH=7.4) with or without glucose (1 mg/mL) as concentration increased. (c) Drug release curves of different nanoparticles over time in PBS (pH=5.0, pH=7.4) with or without glucose (1 mg/mL). (d) changes of size and PDI were tested to evaluate the stability of TPZ/Fe_3O_4@MSN-GOX.

3.5. Detection of hydroxyl radicals

Highly toxic hydroxyl radicals (•OH) depends on the weak acid environment, Fe_3O_4 catalyzes the high level of H_2O_2 produced in the weak acid environment tumor microenvironment[15]. Methylene blue was typical indicator of •OH, which could react with methylene blue to generate colorless product and could be quantitative detected by UV-Vis absorption at 665 nm. In **Figure 7 (a)**, compared with the absorption spectra of methylene blue, the absorption spectra of glucose-free methylene blue solution added with Fe_3O_4@MSN and Fe_3O_4@MSN-GOX had a significant decline. However, in methylene blue solution containing glucose (1 mg/mL), the absorption spectra added with Fe_3O_4@MSN-GOX decreased sharply and approximately disappeared in **Figure**

7 (b). Simultaneously, the colors were also lightened with the decrease in absorbance. The result suggested that the nanoparticles we constructed could effectively generate hydroxyl radicals (•OH) and Fe_3O_4@MSN-GOX could enhanced the level of hydroxyl radicals in glucose media due to the reduced pH and enhanced H_2O_2 level aroused by the GOX-driven oxidation reaction.

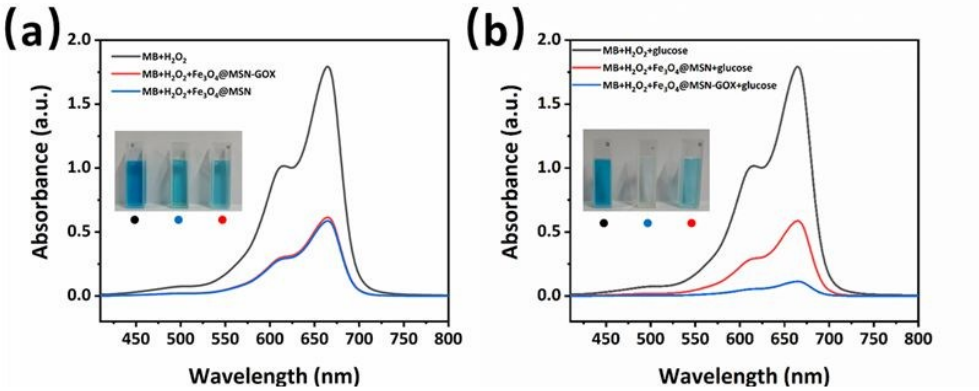

Figure 7. (a) UV-vis absorption spectra and images of MB, MB with Fe_3O_4@MSN and MB with Fe_3O_4@MSN-GOX in glucose-free solutions. (b) UV-vis absorption spectra and images of MB, MB with Fe_3O_4@MSN and MB with Fe_3O_4@MSN-GOX in containing glucose solutions (1 mg/mL).

3.6. Intracellular uptake evaluation

Intracellular distribution of fluorescent TPZ was used to evaluate the uptake of TPZ/Fe_3O_4@MSN-GOX and MCF-7 cells at the density of 1×10^5 cells/dish cultured in DMEM containing 5% CO_2 at 37 ℃ at specific intervals (1h, 4h, 8h) were observed by confocal laser scanning microscopy (CLSM)[7]. Green and blue fluorescence respective came from TPZ and the MCF-7 cell nuclei was stained by DAPI. In **Figure S2**, green fluorescence intensity (TPZ) of TPZ/Fe_3O_4@MSN-GOX in MCF-7 cells had a significant improvement over time, which was attributed to the mechanism that positively charged TPZ/Fe_3O_4@MSN-GOX tended to be endocytosed by negatively overexpressed MCF-7 cells and enhanced permeability and retention (EPR) effect.

View Article Online
DOI: 10.1039/C9NJ05469C

3.7. Reactive oxygen species studies

The intracellular ROS level of TPZ/Fe_3O_4@MSN-GOX was quantitatively detected by the green fluorescent of dichlorofluorescein (DCF), a product of dichlorodihydrofluorescein diacetate (DCFDA) oxidized by ROS. The GOX could remarkably increase the H_2O_2 concentration, which has been proved by previous work. highly toxic ROS was generated by the intracellular superabundant H_2O_2 under the catalysis of Fe^{3+}/Fe^{2+}. Difference of ROS levels induced by TPZ/Fe_3O_4@MSN-GOX, TPZ/Fe_3O_4@MSN at specific interval time (1h, 4h, 8h) in MCF-7 cells was shown in **Figure 8**. Fluorescence intensity of TPZ/Fe_3O_4@MSN-GOX had more obvious improvement in MCF-7 cells than that of TPZ/Fe_3O_4@MSN after 8h, which was attributed to elevated concentration of H_2O_2 aroused by GOX and high level of ROS around by decomposition of H_2O_2 in acid environment. However, only negligible fluorescence signal could be detected in TPZ/Fe_3O_4@MSN in the first 1h, but brighter fluorescence intensity was detected in TPZ/Fe_3O_4@MSN-GOX and significant improvement of the fluorescence intensity of TPZ/Fe_3O_4@MSN-GOX increased as time. The result suggested that TPZ/Fe_3O_4@MSN-GOX we constructed could stimulate highly toxic ROS and revealed the efficient potency in chemodynamic therapy.

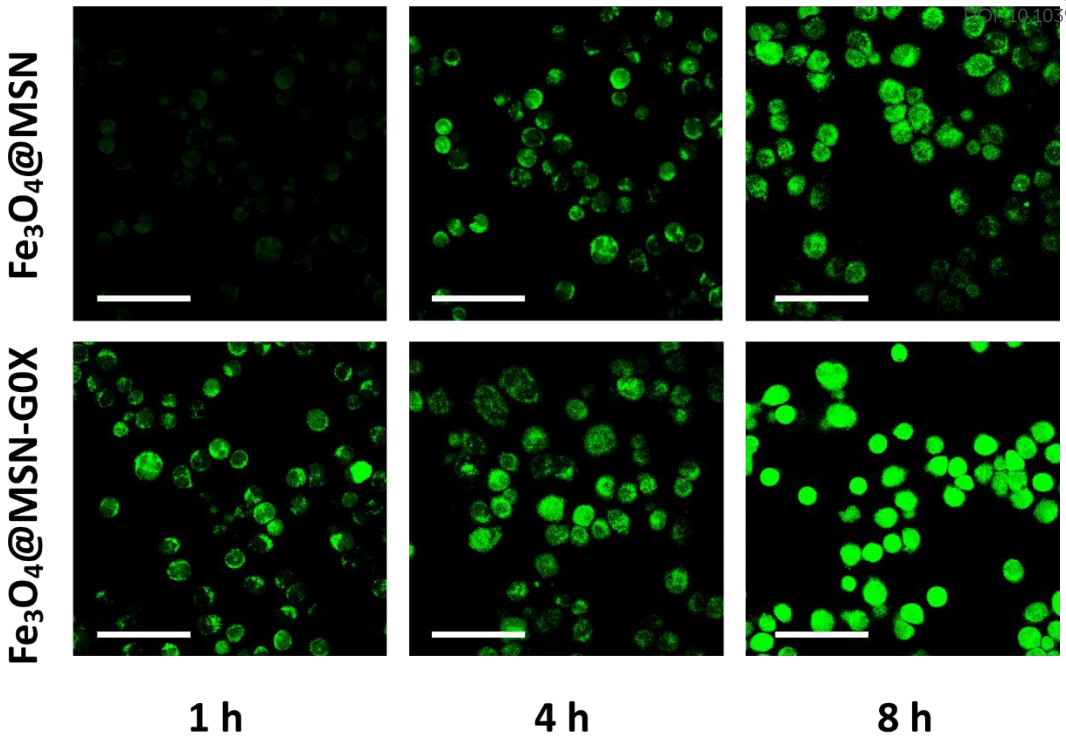

Figure 8. CLSM images of MCF-7 cells incubated with Fe_3O_4@MSN and Fe_3O_4@MSN-GOX for different incubation times. The scale bar is 50 μm.

3.8. In vitro cytotoxicity

GOX induced starvation therapy by depriving glucose and O_2, activated the therapeutic effect of the hypoxia-inducible TPZ and induced highly toxic ROS, which could effectively inhibit tumors. MTT assays was used to demonstrate the toxicities and pharmacological action of nanoparticles toward MCF-7 cells incubated with TPZ/Fe_3O_4@MSN-GOX, TPZ/Fe_3O_4@MSN, free TPZ and control group under different O_2 concentrations in glucose-containing (1 mg/mL). Co-cultured with empty carrier MSN at different concentrations in glucose-containing (1 mg/mL) as control group, the cell viability of MCF-7 cells (20% O_2 concentrations), MCF-7 cells (5% O_2 concentrations) and L-02 cells (20% O_2 concentrations) all exceeded 85% at 200 μg/mL in **Figure 9 (a)**, which was attributed to biocompatibility of MSN and the cytotoxicities of control group was insignificantly influenced by the O_2 concentrations. Starvation therapy triggered by Fe_3O_4@MSN-GOX leaded to the decline of cell viability at the

glucose-containing DMEM media and lower cell viability at a higher concentration of glucose (**Figure S3**), which attributed to the exhaust of glucose and higher level of toxic H_2O_2 production, which was proved in previous work.[39] In glucose-containing (1 mg/mL) with 20% O_2 concentrations, TPZ/Fe_3O_4@MSN-GOX (91.7% cell viability), TPZ/Fe_3O_4@ MSN (93.6% cell viability), TPZ (97.5% cell viability) displayed low level in killing L-02 cells in **Figure 9(b)**, which confirmed the security and biocompatibility to normal cells of nanoparticles we prepared. In normal cells, the O_2 concentrations and pH value are at high level and H_2O_2 concentration is at low level, which meant that hypoxic prodrug TPZ would not be activated and highly toxic hydroxyl radicals would not generate for lack of H_2O_2 and acidic environment. In glucose-containing (1 mg/mL) with 20% O_2 concentrations, TPZ/Fe_3O_4@MSN-GOX (4.7% cell viability) displayed outstanding potency in killing MCF-7 cells than TPZ/Fe_3O_4@MSN (62.1% cell viability) and free TPZ (93.3% cell viability) at TPZ concentrations of 16 μg/mL in **Figure 9(c)**. At high oxygen concentrations, hypoxic-induced TPZ had negligible killing effect on cells. With the participation of GOX, TPZ/Fe_3O_4@MSN-GOX could further reduce the intracellular pH and increase H_2O_2, promoting the production of ROS, while it was difficult for TPZ/Fe_3O_4@MSN to obtain the same effect due to the lack of GOX. GOX and TPZ were loaded into the biocompatible MSN nanoparticles, and TPZ/Fe_3O_4@MSN-GOX could consume glucose and oxygen, provoke spatial control of hypoxia-sensitive TPZ release and cause exacerbated hypoxia. However, in glucose-containing (1 mg/mL) with 5% O_2 concentrations, TPZ/Fe_3O_4@MSN-GOX (8.6% cell viability), TPZ/Fe_3O_4@MSN (29.9% cell viability), TPZ (33.3% cell viability) displayed enhanced potency in inhibiting MCF-7 cells in **Figure 9(d)**, which was attributed to the synergy of starvation therapy, chemodynamic therapy and sensitized chemotherapy, while could not displayed excellent effect for no adequate oxygen triggered sequential multitherapy.

View Article Online
DOI: 10.1039/C9NJ05469C

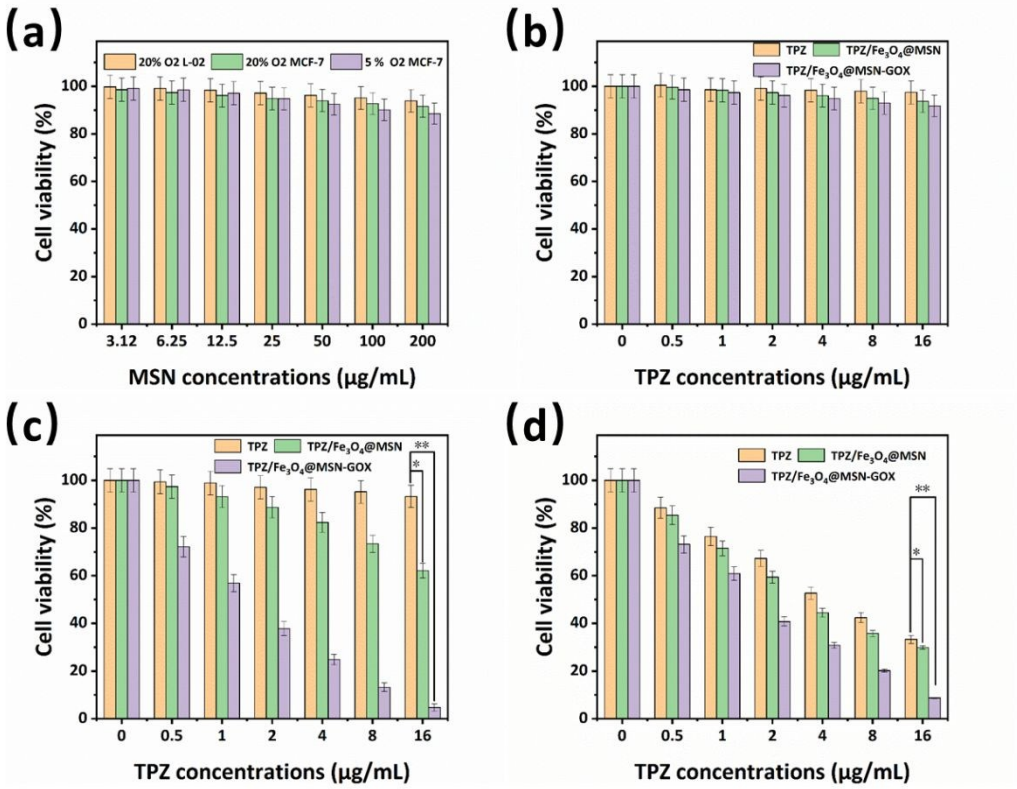

Figure 9. (a) Cells viability rates of different MSN concentrations at different oxygen concentrations. (b) L-02 cells viability rates of different TPZ dose-dependent concentrations of different nanoparticle in 20% O_2 concentration with glucose (1 mg/mL). (c) MCF-7 cells viability rates of different TPZ dose-dependent concentrations of different nanoparticle in 5% O_2 concentration. (d) MCF-7 cells viability rates of different TPZ dose-dependent concentrations of different nanoparticle in 5% O_2 concentration, which treated by different nanoparticles calculated by MTT assay. Data were shown as mean ± S.D. (n=3). Significance is defined as * $P < 0.05$, ** $P < 0.01$

3.9. Cell apoptosis

Cell apoptosis induced by different nanoparticles on MCF-7 cells was detected by flow cytometry with annexin-V-FITC/P assay under different O_2 concentrations (5% and 20%). In **Figure 10**, the apoptosis rates of free TPZ, TPZ/Fe_3O_4@MSN, TPZ/Fe_3O_4@MSN-GOX on MCF-7 cells were respectively 25.3%, 75.7%, 93.4% with

the same TPZ dosage of 40 μg/mL in 20% O_2 and high apoptosis was obtained in 5% O_2, which were 57.4%, 79.5%, 88.2% respectively. 40 μg/mL MSN as the control group exhibited a low apoptotic rate (2.7% in 20% O_2 and 6.0% in 5% O_2), suggesting that it was safe and biocompatible to tissue. TPZ/Fe_3O_4@MSN-GOX displayed better potency in inducing cell apoptosis than free TPZ and TPZ/Fe_3O_4@MSN, attributed to the highly toxic ROS. GOX could elevate the heterogeneity of tumor by reducing pH and enhancing hypoxia, which would sensitize the effect of TPZ and toxic ROS. More important, at high oxygen (20% O_2), GOX could work effectively and produced more H_2O_2 and lower pH, stimulating more highly toxic ROS, which leaded the more apoptosis.

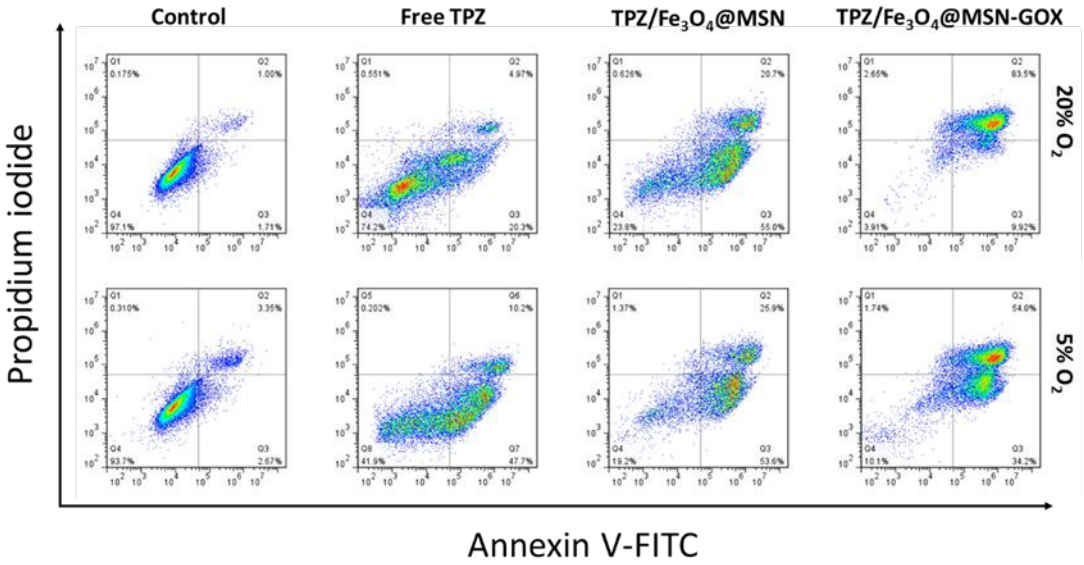

Figure 10. Cell apoptosis induced by control group, free TPZ, TPZ/Fe_3O_4@MSN, TPZ/Fe_3O_4@MSN-GOX at 40 μg/mL TPZ dose-dependent concentrations in a normoxic (20% O_2) and hypoxic (5% O_2) environment for 12h.

Conclusion

In summary, multimodal therapies based on synergy of starvation therapy, chemotherapy and chemodynamic therapy was introduced for efficient cancer therapy. A novel drug delivery system (TPZ/Fe_3O_4@MSN-GOX) was successful constructed, which characterized by FT-IR, UV-vis spectrometry, TEM, SEM, TGA and DLS and possessed uniformly dispersed size, distinct pore structure with highly drug loading and

stability. The result revealed that GOX could reduce pH and elevate H_2O_2 concentration. Reduced pH could accelerate the release of TPZ and iron ion were proved by vitro experiment. Abundant hydroxyl radicals were generated by Fe_3O_4@MSN-GOX, which detected by the color and UV-vis absorption changes of MB. Obvious increasing in ROS level of MCF-7 cells were detected when was co-cultured with Fe_3O_4@MSN-GOX in normoxic environment containing glucose. Multifunctional TPZ/Fe_3O_4@MSN-GOX nanoparticle was also revealed high cellular uptake capacity, excellent inhibitory effect and cell apoptosis on MCF-7 cells, which would have great prospects in the field of cancer therapy.

Acknowledgments

We are highly grateful to the International S&T Cooperation Program of China (No. 2015DFG42240), the financial support from the National Natural Science Foundation of China (Grant Nos. 21628101 and 21371031), the project funded by China Postdoctoral Science Foundation (NO. 2019M651841), the Priority Academic Program Development (PAPD) of Jiangsu Higher Education Institutions and State Key Laboratory of Bioelectronics-Zhongda Hospital cross innovation cooperation research fund (No. 2018yy-jccx012)

Author Information

Corresponding Author

Baiwang Sun; E-mail address: chmsunbw@seu.edu.cn

Notes

The authors declare no competing financial interest. All experiments in this research work complied with the Regulations on the Administration of Laboratory Animals and

View Article Online
DOI: 10.1039/C9NJ05469C

the relevant national laws and regulations and were performed under the guidance approved by the Laboratory Animal Ethics Committee at the School of Medicine, Southeast University (Nanjing, China).

References

(1) Gao, Z.; Li, Y.; You, C.; Sun, K.; An, P.; Sun, C.; Wang, M.; Zhu, X.; Sun, B. Iron Oxide Nanocarrier-Mediated Combination Therapy of Cisplatin and Artemisinin for Combating Drug Resistance through Highly Increased Toxic Reactive Oxygen Species Generation. *ACS Appl. Bio Mater.* **2018**, *1*, 270–280.

(2) Lee, E. S.; Na, K.; Bae, Y. H. Polymeric micelle for tumor pH and folate-mediated targeting. *Journal of Controlled Release* **2003**, *91*, 103–113.

(3) Li, Y.; Gao, Z.; Chen, F.; You, C.; Wu, H.; Sun, K.; An, P.; Cheng, K.; Sun, C.; Zhu, X. *et al.* Decoration of Cisplatin on 2D Metal-Organic Frameworks for Enhanced Anticancer Effects through Highly Increased Reactive Oxygen Species Generation. *ACS Appl. Mater. Interfaces.* **2018**, *10*, 30930–30935.

(4) Zhang, M.-K.; Li, C.-X.; Wang, S.-B.; Liu, T.; Song, X.-L.; Yang, X.-Q.; Feng, J.; Zhang, X.-Z. Tumor Starvation Induced Spatiotemporal Control over Chemotherapy for Synergistic Therapy. *Small* **2018**, *14*, e1803602.

(5) Wang, Y.; Song, S.; Liu, J.; Liu, D.; Zhang, H. ZnO-Functionalized Upconverting Nanotheranostic Agent: Multi-Modality Imaging-Guided Chemotherapy with On-Demand

View Article Online
DOI: 10.1039/C9NJ05469C

Drug Release Triggered by pH. *Angew. Chem. Int. Ed.* **2015**, *54*, 536–540.

(6) Fu, L.-H.; Qi, C.; Hu, Y.-R.; Lin, J.; Huang, P. Glucose Oxidase-Instructed Multimodal Synergistic Cancer Therapy. *Adv. Mater.* **2019**, *0*, 1808325.

(7) Huang, L.; Liu, J.; Gao, F.; Cheng, Q.; Lu, B.; Zheng, H.; Xu, H.; Xu, P.; Zhang, X.; Zeng, X. A dual-responsive, hyaluronic acid targeted drug delivery system based on hollow mesoporous silica nanoparticles for cancer therapy. *J. Mater. Chem. B* **2018**, *6*, 4618–4629.

(8) Sun, K.; Gao, Z.; Zhang, Y.; Wu, H.; You, C.; Wang, S.; An, P.; Sun, C.; Sun, B. Enhanced highly toxic reactive oxygen species levels from iron oxide core–shell mesoporous silica nanocarrier-mediated Fenton reactions for cancer therapy. *J. Mater. Chem. B* **2018**, *6*, 5876–5887.

(9) Shi, C.; Liu, T.; Guo, Z.; Zhuang, R.; Zhang, X.; Chen, X. Reprogramming Tumor-Associated Macrophages by Nanoparticle-Based Reactive Oxygen Species Photogeneration. *Nano lett.* **2018**, *18*, 7330–7342.

(10) Wang, S.; Wang, Z.; Yu, G.; Zhou, Z.; Jacobson, O.; Liu, Y.; Ma, Y.; Zhang, F.; Chen, Z.-Y.; Chen, X. Tumor-Specific Drug Release and Reactive Oxygen Species Generation for Cancer Chemo/Chemodynamic Combination Therapy. *Adv. Sci.* **2019**, *6*, 1801986.

(11) Liu, C.; Wang, D.; Zhang, S.; Cheng, Y.; Yang, F.; Xing, Y.; Xu, T.; Dong, H.; Zhang, X. Biodegradable Biomimic Copper/Manganese Silicate Nanospheres for Chemodynamic/Photodynamic Synergistic Therapy with Simultaneous Glutathione Depletion and Hypoxia Relief. *ACS Nano* **2019**, *13*, 4267–4277.

View Article Online
DOI: 10.1039/C9NJ05469C

(12) Jeong, D.; Bae, B.-c.; Park, S.-j.; Na, K. Reactive oxygen species responsive drug releasing nanoparticle based on chondroitin sulfate–anthocyanin nanocomplex for efficient tumor therapy. *Journal of Controlled Release* **2016**, *222*, 78–85.

(13) Tang, Z.; Liu, Y.; He, M.; Bu, W. Chemodynamic Therapy: Tumour Microenvironment-Mediated Fenton and Fenton-like Reactions. *Angew. Chem. Int. Ed.* **2019**, *58*, 946–956.

(14) Wu, H.; You, C.; Chen, F.; Jiao, J.; Gao, Z.; An, P.; Sun, B.; Chen, R. Enhanced cellular uptake of near-infrared triggered targeted nanoparticles by cell-penetrating peptide TAT for combined chemo/photothermal/photodynamic therapy. *Materials Science and Engineering: C* **2019**, *103*, 109738.

(15) Huo, M.; Wang, L.; Chen, Y.; Shi, J. Tumor-selective catalytic nanomedicine by nanocatalyst delivery. *Nature communications* **2017**, *8*, 357.

(16) Wang, Y.; Yin, W.; Ke, W.; Chen, W.; He, C.; Ge, Z. Multifunctional Polymeric Micelles with Amplified Fenton Reaction for Tumor Ablation. *Biomacromolecules* **2018**, *19*, 1990–1998.

(17) Yang, Y.; Yang, X.; Li, H.; Li, C.; Ding, H.; Zhang, M.; Guo, Y.; Sun, M. Near-infrared light triggered liposomes combining photodynamic and chemotherapy for synergistic breast tumor therapy. *Colloids and surfaces. B, Biointerfaces* **2019**, *173*, 564–570.

(18) Zhang, L.; Wan, S.-S.; Li, C.-X.; Xu, L.; Cheng, H.; Zhang, X.-Z. An Adenosine Triphosphate-Responsive Autocatalytic Fenton Nanoparticle for Tumor Ablation with Self-Supplied H2O2 and Acceleration of Fe(III)/Fe(II) Conversion. *Nano lett.* **2018**, *18*, 7609–

View Article Online
DOI: 10.1039/C9NJ05469C

7618.

(19) Gao, S.; Lin, H.; Zhang, H.; Yao, H.; Chen, Y.; Shi, J. Nanocatalytic Tumor Therapy by Biomimetic Dual Inorganic Nanozyme-Catalyzed Cascade Reaction. *Adv. Sci.* **2019**, *6*, 1801733.

(20) Gao, Z.; Li, Y.; You, C.; Sun, K.; An, P.; Sun, C.; Wang, M.; Zhu, X.; Sun, B. Iron Oxide Nanocarrier-Mediated Combination Therapy of Cisplatin and Artemisinin for Combating Drug Resistance through Highly Increased Toxic Reactive Oxygen Species Generation. *ACS Appl. Bio Mater.* **2018**, *1*, 270–280.

(21) Fan, J.-X.; Peng, M.-Y.; Wang, H.; Zheng, H.-R.; Liu, Z.-L.; Li, C.-X.; Wang, X.-N.; Liu, X.-H.; Cheng, S.-X.; Zhang, X.-Z. Engineered Bacterial Bioreactor for Tumor Therapy via Fenton-Like Reaction with Localized H2O2 Generation. *Adv. Mater.* **2019**, *31*, 1808278.

(22) Giannakis, S.; Voumard, M.; Rtimi, S.; Pulgarin, C. Bacterial disinfection by the photo-Fenton process: Extracellular oxidation or intracellular photo-catalysis? *Applied Catalysis B: Environmental* **2018**, *227*, 285–295.

(23) Fan, W.; Lu, N.; Huang, P.; Liu, Y.; Yang, Z.; Wang, S.; Yu, G.; Liu, Y.; Hu, J.; He, Q. *et al.* Glucose-Responsive Sequential Generation of Hydrogen Peroxide and Nitric Oxide for Synergistic Cancer Starving-Like/Gas Therapy. *Angew. Chem. Int. Ed.* **2017**, *56*, 1229–1233.

(24) Fu, L.-H.; Qi, C.; Lin, J.; Huang, P. Catalytic chemistry of glucose oxidase in cancer diagnosis and treatment. *Chem. Soc. Rev.* **2018**, *47*, 6454–6472.

(25) Liang, R.; Chen, Y.; Huo, M.; Zhang, J.; Li, Y. Sequential catalytic nanomedicine

augments synergistic chemodrug and chemodynamic cancer therapy. *Nanoscale Horiz.* **2019**, *46*, 7021.

(26) Zhang, Y.; Yang, Y.; Jiang, S.; Li, F.; Lin, J.; Wang, T.; Huang, P. Degradable silver-based nanoplatform for synergistic cancer starving-like/metal ion therapy. *Mater. Horiz.* **2019**, *6*, 169–175.

(27) Cui, Q.; Wang, J.-Q.; Assaraf, Y. G.; Ren, L.; Gupta, P.; Wei, L.; Ashby, C. R.; Yang, D.-H.; Chen, Z.-S. Modulating ROS to overcome multidrug resistance in cancer. *Drug Resistance Updates* **2018**, *41*, 1–25.

(28) Stella, V. J.; Nti-Addae, K. W. Prodrug strategies to overcome poor water solubility. *Adv. Drug Deliver. Rev.* **2007**, *59*, 677–694.

(29) Verheggen, I.C.M.; van Boxtel, M.P.J.; Verhey, F.R.J.; Jansen, J.F.A.; Backes, W. H. Interaction between blood-brain barrier and glymphatic system in solute clearance. *Neurosci. Biobehav. Rev.* **2018**, *90*, 26–33.

(30) Gao, Z.; You, C.; Wu, H.; Wang, M.; Zhang, X.; Sun, B. FA and cRGD dual modified lipid-polymer nanoparticles encapsulating polyaniline and cisplatin for highly effective chemo-photothermal combination therapy. *J. Biomat. Sci-Polym. E.* **2018**, *29*, 397–411.

(31) Hu, M.; Ju, Y.; Liang, K.; Suma, T.; Cui, J.; Caruso, F. Void Engineering in Metal-Organic Frameworks via Synergistic Etching and Surface Functionalization. *Adv. Funct. Mater.* **2016**, *26*, 5827–5834.

(32) Johnson, C. M.; Pate, K. M.; Shen, Y.; Viswanath, A.; Tan, R.; Benicewicz, B. C.; Moss, M. A.; Greytak, A. B. A methacrylate-based polymeric imidazole ligand yields quantum dots with low cytotoxicity and low nonspecific binding. *Journal of Colloid and*

View Article Online
DOI: 10.1039/C9NJ05469C

Interface Science **2015**, *458*, 310–314.

(33) Chu, D.; Dong, X.; Shi, X.; Zhang, C.; Wang, Z. Neutrophil-Based Drug Delivery Systems. *Adv. Mater.* **2018**, *30*, 1706245.

(34) Sun, K.; You, C.; Wang, S.; Gao, Z.; Wu, H.; Tao, W. A.; Zhu, X.; Sun, B. NIR stimulus-responsive core-shell type nanoparticles based on photothermal conversion for enhanced antitumor efficacy through chemo-photothermal therapy. *Nanotechnology* **2018**, *29*, 285302.

(35) Zhao, Q.; Liu, J.; Zhu, W.; Sun, C.; Di, D.; Zhang, Y.; Wang, P.; Wang, Z.; Wang, S. Dual-stimuli responsive hyaluronic acid-conjugated mesoporous silica for targeted delivery to CD44-overexpressing cancer cells. *Acta biomaterialia* **2015**, *23*, 147–156.

(36) Jang, B.; Kwon, H.; Katila, P.; Lee, S. J.; Lee, H. Dual delivery of biological therapeutics for multimodal and synergistic cancer therapies. *Adv. Drug Delivery Rev.* **2016**, *98*, 113–133.

(37) Nyalosaso, J. L.; Rascol, E.; Pisani, C.; Dorandeu, C.; Dumail, X.; Maynadier, M.; Gary-Bobo, M.; Kee Him, J. L.; Bron, P.; Garcia, M. *et al.* Synthesis, decoration, and cellular effects of magnetic mesoporous silica nanoparticles. *RSC Adv.* **2016**, *6*, 57275–57283.

(38) Gao, Z.; Shi, T.; Li, Y.; You, C.; Cheng, K.; Sun, B. Mesoporous silica-coated gold nanoframes as drug delivery system for remotely controllable chemo-photothermal combination therapy. *Colloids and surfaces. B, Biointerfaces* **2019**, *176*, 230–238.

(39) Cheng, K.; Zhang, Y.; Li, Y.; Gao, Z.; Chen, F.; Sun, K.; An, P.; Sun, C.; Jiang, Y.; Sun, B. A novel pH-responsive hollow mesoporous silica nanoparticle (HMSN) system

View Article Online
DOI: 10.1039/C9NJ05469C

encapsulating doxorubicin (DOX) and glucose oxidase (GOX) for potential cancer treatment. *J. Mater. Chem. B* **2019**, *15*, 3603.

(40) Jiao, S.; Li, Y.; Gao, Z.; Chen, R.; Wang, Y.; Zou, Z. The synthesis of an antifungal 1,2,4-triazole drug and the establishment of a drug delivery system based on zeolitic imidazolate frameworks. *New J. Chem.* **2019**, *43*, 18823–18831.

(41) You, C.-Q.; Wu, H.-S.; Gao, Z.-G.; Sun, K.; Chen, F.-H.; Tao, W. A.; Sun, B.-W. Subcellular co-delivery of two different site-oriented payloads based on multistage targeted polymeric nanoparticles for enhanced cancer therapy. *J. Mater. Chem. B* **2018**, *6*, 6752–6766.

(42) Jin, R.; Liu, Z.; Bai, Y.; Zhou, Y.; Gooding, J. J.; Chen, X. Core-Satellite Mesoporous Silica-Gold Nanotheranostics for Biological Stimuli Triggered Multimodal Cancer Therapy. *Adv. Funct. Mater.* **2018**, *28*, 1801961.